Supplement of Earth Surf. Dynam., 12, 819–839, 2024
https://doi.org/10.5194/esurf-12-819-2024-supplement

Earth Surface Dynamics
Open Access
EGU

Supplement of

Role of the forcing sources in morphodynamic modelling of an embayed beach

Nil Carrion-Bertran et al.

Correspondence to: Nil Carrion-Bertran (nil.carrion@upc.edu) and Francesca Ribas (francesca.ribas@upc.edu)

In this Supplementary Information document, four sections are included. Sect. S1 contains an extra figure with ortomosaic aereal pictures of the study site. Sect. S2 describes the methodology implemented to propagate wave conditions from the Cap Begur buoy to the AWAC location using the SWAN model. Sect. S3 includes the description of the two morphodynamic models used, XBeach and Q2Dmorfo. Finally, Sect. S4 contains additional figures that illustrate the calibration process of the two models using Castell beach data.

S1 Ortomosaic aereal pictures

In order to visualize the changes in the dry beach during he 6 month studied, ortomosaic aereal images of the initial and final dates are shown in Fig. S1. These changes are not reproduced by the models, as explained in the main text, because the corresponding physical processes are not included.

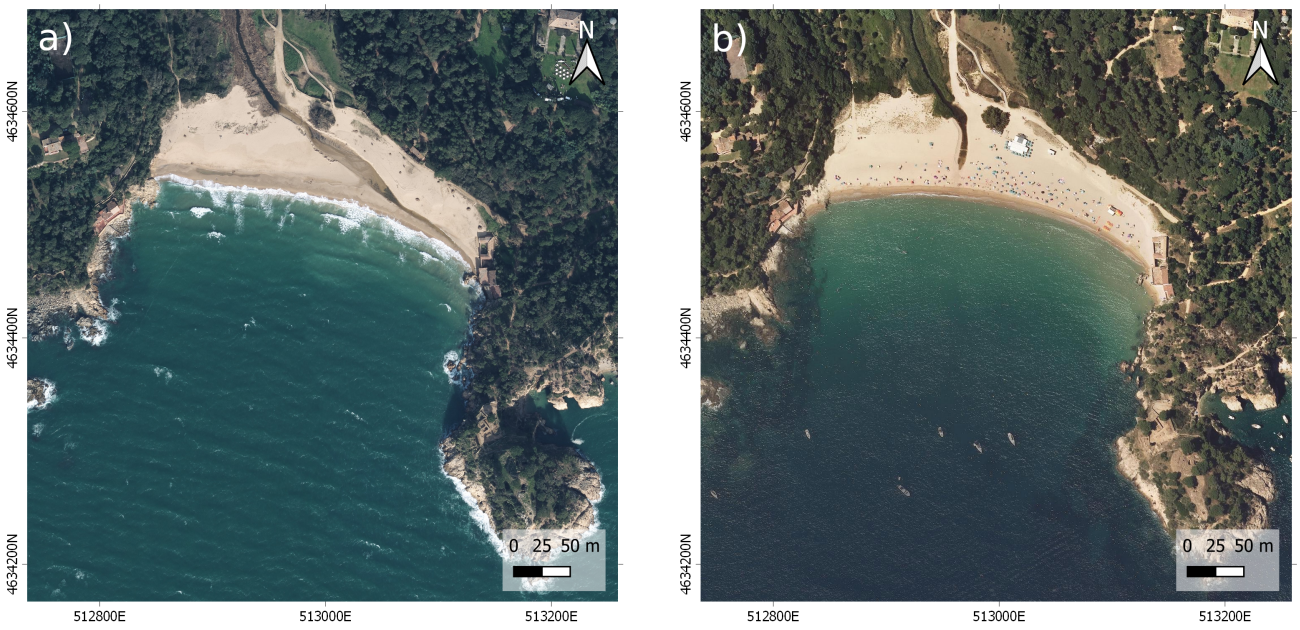

Figure S1. Ortomosaic aereal pictures from Castell beach. Panel (a) (left) was obtained the 27th of January 2020 and the panel (b) (right) was obtained between the 27th of May to the 8th of July of 2020. Images obtained from Institut Cartogràfic i Geològic de Catalunya (ICGC).

S2 Description of the wave propagation method

One of the wave datasets used as boundary condition in the morphodynamic models was obtained by propagating wave data measured by an offshore wave buoy to a location in front of the study site using the SWAN model (AWAC position). This appendix provides additional details regarding the wave propagation model setup and validation.

S2.1 Model setup

SWAN (Simulating Waves Nearshore) is a third-generation spectral wave model that computes the evolution of the 2D frequency-direction wave spectrum in coastal regions and inland waters (Team, 2019a).

The SWAN Cycle III version 41.31 code (Team, 2019b) was used to propagate the wave conditions measured by the Cap Begur wave buoy (located at 3.65°E 41.9°N at a water depth of 1200 m, Fig. S2) to the AWAC location (at 14.5 m depth), following a methodology similar to De Swart et al. (2020). The model domain consists of a main rectangular grid that stretches approximately 70 km alongshore and 35 km cross-shore and has a spatial resolution of approximately 300 m (Fig. S2a). Within the main grid, three additional rectangular grids are nested to increase the resolution (each with a factor 3), resulting in a spatial resolution of approximately 10 m around Castell beach (Fig. S2c). Bathymetric data was obtained from different surveys and has a resolution of 25m in the model domain, except in the area adjacent to Castell beach (within a radius of about 1.5 km), where the resolution is 5m (Fig. S2b, d). SWAN was used in 2D non-stationary mode and stationary computations (recommended for domains smaller than 1 deg) with a maximum of 50 iterations per computation were employed. The frequency space consisted of 38 logarithmically spaced values in the range 0.03–1 Hz, with the recommended frequency resolution of df/f = 0.1 (Team, 2019b) and the directional resolution was 5°. For bottom friction, the default JONSWAP formulation was used with a coefficient value of 0.038 m2s-3. The default third-generation physics formulation of Komen et al. (1984) was used (including wave decay due to whitecapping) with constant wave breaking (alpha = 1 and gamma = 0.73), whilst quadruplets, triad wave-wave interactions and wave growth by wind were switched off.

S2.2 Boundary conditions

Following De Swart et al. (2020), full 2D frequency-direction spectra of the sea-surface elevation variance, $E(f,\theta)$, were specified as boundary conditions. Unfortunately, the Cap Begur wave buoy did not measure the full spectra $E(f,\theta)$, but it did provide the sea-surface elevation variance E, mean direction θ_m and directional spreading $\sigma\theta$ for a total of 14 spectral bands. This data was used to reconstruct $E(f,\theta)$ using the 1D frequency spectrum $E(f)$ and the directional distribution $D(f,\theta)(E(f,\theta) = E(f)D(f,\theta))$. Here, $E(f)$ was determined directly from the buoy variance data and $D(f,\theta)$ was computed from the directional properties using the cos^{2s} method (Mitsuyasu et al., 1975). The resulting 2D frequency-direction spectra were imposed along the entire southeastern and northeastern boundaries, and parts of the southwestern and northwestern boundaries (Fig. S2a), meaning that they were assumed to be spatially constant and equal to those at the Cap Begur buoy.

S2.3 Model validation

The SWAN results at Castell beach were validated using the AWAC measurements. An overview of the statistical errors for various wave parameters and different wave climates is given in Table S1. Modelled wave height and period agree well with the measurements, whilst larger differences are found between the modelled and measured mean wave direction. The largest errors for all wave parameters are encountered during northerly waves, but fortunately these waves are not that important for studying the morphological evolution of Castell beach. The southern orientation of the coastline at Castell beach and the headlands' presence ensures that northerly waves undergo substantial refraction (well over 90 °) to reach Castell beach so that their energy is considerably reduced (Fig. S3). For the other wave climates, the errors in the various wave parameters are much smaller (Table S1). In conclusion, the validation results show that the SWAN model is well-capable of propagating measured offshore wave conditions to Castell beach that can subsequently be used as input for morphodynamic models.

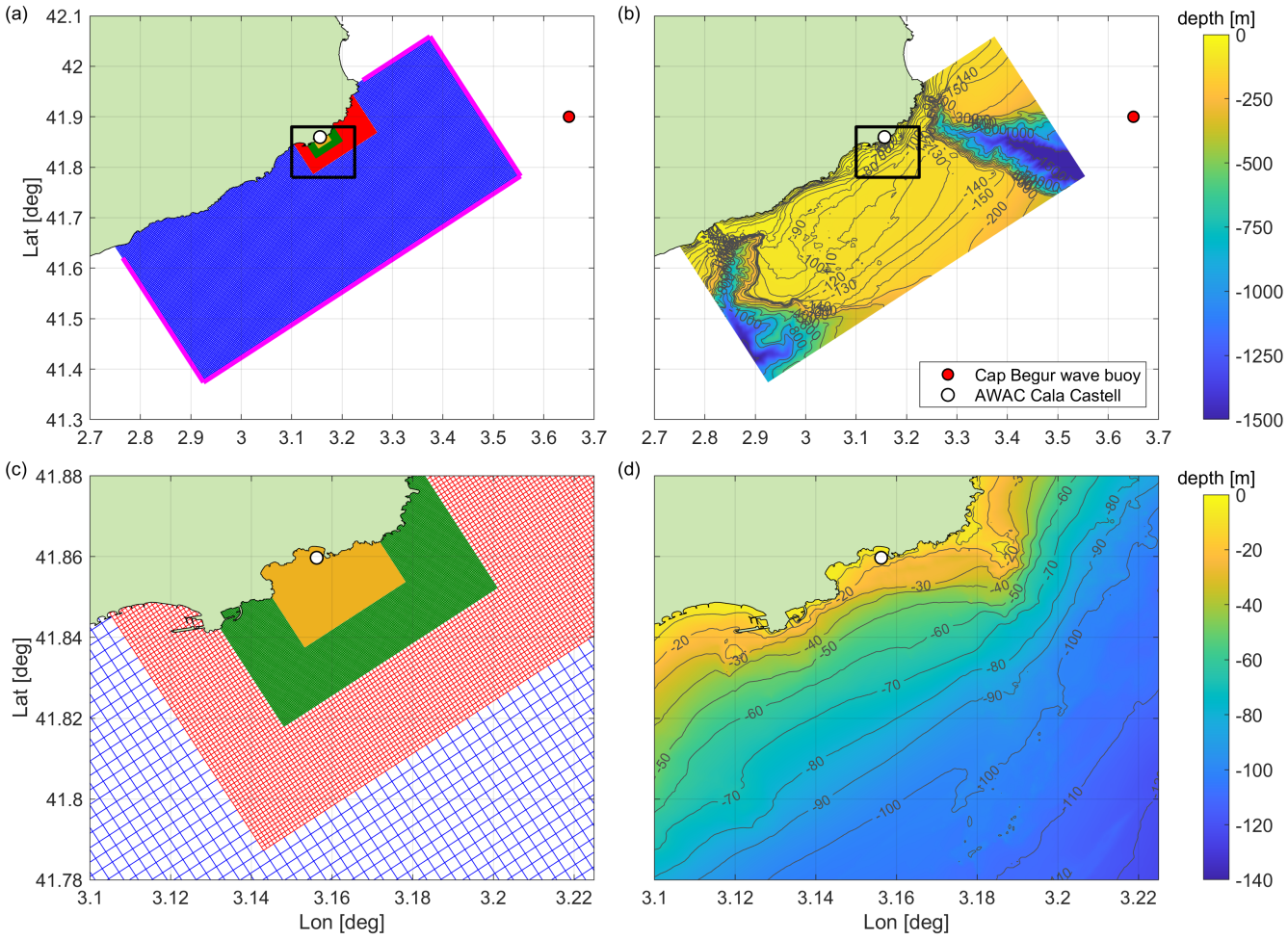

Figure S2. Overview of the model domain for the SWAN simulations including the locations of Cap Begur wave buoy and the AWAC at Castell beach. Panel (a) shows the main grid in blue and the three nested grids in red, green and yellow, as well as the boundary sections where wave conditions were imposed in magenta. Panel (b) shows the model bathymetry in the entire model domain. Panels (c) and (d) are identical to panels (a) and (b), but show a zoom of the area around Castell beach (displayed area is indicated by the black square in panels (a) and (b)).

Table S1. Comparison of the SWAN simulations results with the AWAC measurements for different wave parameters and wave climates. The wave climates were determined from the full 2D frequency-direction spectra of the Begur buoy.

	H_{m0} $[m]$		T_{m02} $[s]$		θ_m $[deg]$	
	RMSE	BIAS	RMSE	BIAS	RMSE	BIAS
Full period	0.15	-0.08	0.92	0.32	21.5	2.8
Northerly	0.21	-0.17	1.32	0.74	29.4	-13.6
Easterly	0.16	-0.08	0.92	0.53	12.4	8.4
Southwesterly	0.16	-0.02	0.74	0.54	18.1	12.4
Bimodal	0.11	-0.04	0.69	-0.03	20.1	6.4

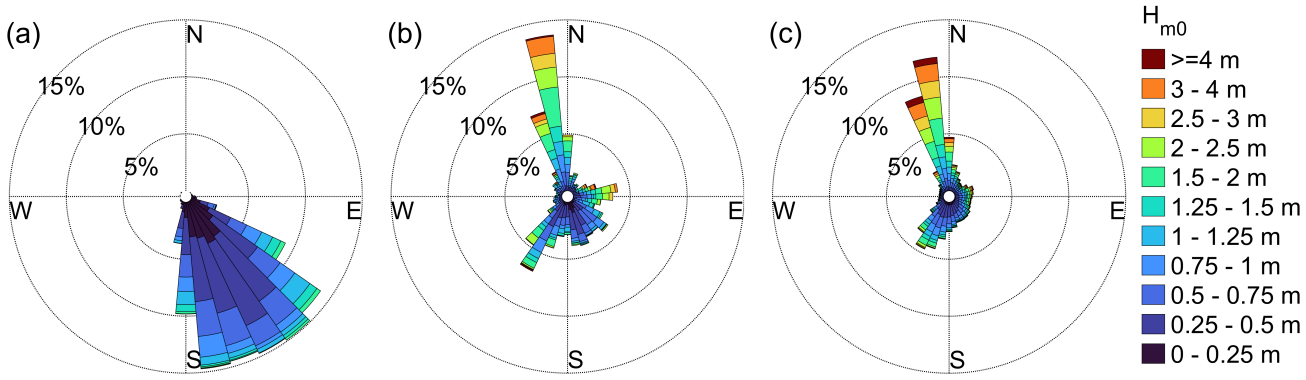

Figure S3. Wave roses of the wave climate measured by the Castell beach AWAC between 28 January 2020 and 8 July 2020 (a), the Cap Begur wave buoy during the AWAC deployment (b) and at the Cap Begur wave buoy between April 2001 and October 2022 (c).

S3 Detailed information of XBeach and Q2Dmorfo models

S3.1 XBeach equations

The model propagates the short waves using the time-dependent wave-action balance equation and the roller equation. In these equations, the directional distribution of the wave-action density is taken into account, whereas the frequency spectrum is characterized by a single representative value. Three wave modes are implemented in XBeach. The `stationary` one resolves the wave-averaged equations, without including the infragravity waves associated to the short wave action. In the present application, this mode presented a systematic erosion in the surf zone inducing an unrealistic recession of the coastline (compared to the final measured topobathymetry). There is also a non-stationary mode called `surfbeat`, that simulates the short wave variations on the wave group scale and their associated long waves. Using this mode, in agreement with the literature (Rutten et al., 2021; Bae et al., 2022), is it possible to simulate the beach response to the incoming waves with a more realistic onshore transport in the surf zone minimising the shoreline recession. The third mode is the `non-hydrostatic` one, which resolves individual waves, but it was discarded in this study due to its high computational cost.

XBeach generates random wave time series within the spectral wave boundary condition that include wave groupiness, only when the `surfbeat` mode is used. Then, waves entering the domain are slightly different for each particular simulation, even when running exactly with the same model setup, imitating the stochastic nature of a real sea. In fact, this only occurs if a XBeach parameter called `random` equals 1. This of course affects beach dynamics: since the incident waves slightly change in each "particular simulation", the sediment transport is also modified, and the beach response can be different with exactly the same model setup. These small changes can accumulate over time and become significant when a large period of time is simulated, like in the present study. The effect of the `random` parameter was hardly evaluated in previous studies because either shorter time periods were simulated or this randomness was simply disabled (`random`$= 0$) and therefore the same wave time series was always applied. In Rutten et al. (2021) the `random` mode was enabled and they demonstrated the importance of including wave stochastic behaviour for the morphodynamic evolution of a beach. Using `random`$= 0$ only reproduces a specific offshore wave condition that leads to a particular result, which might not be representative to the real stochastic character of the waves propagating to the shore, and does not take into account other potential realizations.

The low-frequency currents and sea surface levels are determined using the nonlinear shallow water momentum and mass balance equations, using a Generalized Lagrangian Mean formulation and including all relevant forces (e.g., wind, waves, bed friction and turbulent diffusivity). The main dynamic variables are the water depth D and the depth-averaged water velocity $\boldsymbol{v}^L$, which is called Lagrangian velocity in XBeach terminology. The model also uses a second velocity (called Eulerian in their terminology), $\boldsymbol{v}^E = \boldsymbol{v}^L - \boldsymbol{v}^S$, which is the depth-averaged velocity minus the Stokes drift velocity $\boldsymbol{v}^S$, computed out of the wave and roller energies (van Thiel de Vries, 2009). Bed shear stresses are computed using the formulation by Ruessink et al. (2001), written as a function of the velocity $\boldsymbol{v}^E$ (for being more representative of the current near the bed) and the bottom friction coefficient, c_f. The latter is modelled using the depth-dependant Manning formulation, $c_f = g\,n^2/D^{1/3}$, where g is gravity and n is a coefficient that can be varied.

An advection-diffusion equation (Galappatti and Vreugdenhil, 1985) is solved to compute the depth-averaged sediment volumetric concentration c,

$$\frac{\partial(c\,D)}{\partial t} + \nabla\cdot\Big(c\,D\,(\boldsymbol{v}^E + u^A\hat{k}) + \nu_h\,D\,\nabla c\Big) = D\,\frac{c_{eq}-c}{T_s}\;, \tag{S1}$$

Here, u^A is a velocity magnitude representing the wave nonlinearity, $\hat{k}$ is the wave direction and ν_h is the horizontal eddy viscosity that is used both here to represent a sediment diffusion coefficient and in the water momentum balance. The wave nonlinearity velocity is expressed as

$$u^A = (f_{Sk}\,S_k - f_{As}\,A_s)\,u_{rms}\;, \tag{S2}$$

where S_k and A_s describe the skewness and asymmetry in wave motion, respectively (computed following van Thiel de Vries (2009)), u_{rms} is the standard RMS wave orbital velocity near the bed and f_{Sk} and f_{As} are two important calibration parameters. Moreover, c_{eq} in the RHS of Eq. (S1) is the depth-averaged equilibrium sediment concentration and T_s is an adaptation time

(for the concentration to reach the equilibrium value) computed as a function of water depth and sediment fall velocity (van Thiel de Vries, 2009). Several formulations can be used for c_{eq} and we chose the XBeach default one, the Van Thiel-Van Rijn equation, which reads

$$c_{eq} = \frac{A_{sb}}{D}\left(\sqrt{|\boldsymbol{v}^E|^2 + 0.64(u_{rms}^2 + 1.45k_b)} - u_{cr}\right)^{1.5} + \frac{A_{ss}}{D}\left(\sqrt{|\boldsymbol{v}^E|^2 + 0.64(u_{rms}^2 + 1.45k_b)} - u_{cr}\right)^{2.4}, \tag{S3}$$

where A_{sb} and A_{ss} are the bed load and suspended load parameters (van Thiel de Vries, 2009) and u_{cr} is the critical velocity, computed as a weighted summation of the separate contributions by currents and waves. The sediment is assumed to be stirred by currents, waves and turbulence, where k_b is the near-bed turbulence energy. The latter is an important source of sediment resuspension under breaking waves (Ribas et al., 2011) and is modelled following Roelvink and Stive (1989).

Finally, the seabed evolution is computed by solving the Exner equation,

$$\frac{\partial z_b}{\partial t} + \frac{f_{mor}}{1-p}\nabla\cdot\boldsymbol{q} = 0\,, \tag{S4}$$

where z_b is the bed level, f_{mor} is the morphological acceleration factor, $p = 0.4$ is the porosity, and $\boldsymbol{q}$ is the total volumetric flux (or transport) of sediment and reads

$$\boldsymbol{q} = c\,D\left(\boldsymbol{v}^E + u^A\hat{k}\right) + \nu_h\,D\,\nabla c\; - f_{sl}\,c\,D\,|\boldsymbol{v}^L|\,\nabla z_b. \tag{S5}$$

The last term represents the bed slope effect with f_{sl} being the corresponding parameter. Notice that equations (S1), (S3), (S4) and (S5) must be consistent with the conservation of sediment. This only occurs if $\frac{\partial(c\,D)}{\partial t} = 0$ but, since this term is typically small, the error committed is minor. Besides, a reference bed slope of the swash zone, β_s, can also be provided so that the swash zone profile tends towards it where $H/D > 1$, when working in `surfbeat` mode. Finally, an avalanching algorithm is also used in XBeach to account for the sediment collapse occurring during storm-induced dune erosion (Roelvink et al., 2009).

S3.2 Q2Dmorfo equations

The model solves Eq. (S4), with $p = 0.4$ and $f_{mor} = 1$, to compute the evolution of the bed level. The total volumetric flux of sediment $\boldsymbol{q}$ is assumed to be composed of longshore $\boldsymbol{q_L}$, cross-shore $\boldsymbol{q_C}$ and diffusive $\boldsymbol{q_D}$ components,

$$\boldsymbol{q} = \boldsymbol{q_L} + \boldsymbol{q_C} + \boldsymbol{q_D}\,. \tag{S6}$$

At each point, the local "cross-shore" direction is defined by a unit vector $\hat{\mathbf{n}}$ perpendicular to a local smoothed bathymetric contour and directed offshore (see Arriaga et al. (2017) for details), and the local mean "alongshore" direction $\hat{\mathbf{t}}$ is defined so that the local system is orthonormal and right-handed.

The first term in Eq. (S6) is the sediment transport related with the wave-induced longshore current and it is based on the CERC formula (Komar, 1998)

$$\boldsymbol{q_L} = \mu\,H_b^{5/2}\left(\sin(2\alpha_b) - \frac{2r}{\beta_c}\cos(\alpha_b)\frac{\partial H_b}{\partial x}\right) f(y')\,\hat{\mathbf{t}}\,, \tag{S7}$$

where H_b is the RMS wave height at breaking, $\alpha_b = \theta_b - \phi_s$ is the angle between the wave direction at breaking and the local shore normal, and μ is a calibration parameter which is proportional to the standard CERC constant K (Arriaga et al., 2017). The additional term proportional to the gradient of H_b is relatively uncommon but has been here included to account for the alongshore gradients in wave setup and is controlled by the r parameter (Horikawa, 1988). Finally, $f(y')$ is a normalized cross-shore shape function, assumed to mimic the longshore current profile. Here, y' is the distance from the closest coastline location to the point and β_c is the actual beach slope at the shoreline. The second term in Eq. (S6) parameterises the cross-shore

transport by assuming a bathymetric tendency to evolve to a prescribed alongshore-uniform equilibrium profile, with $\boldsymbol{q_C}$ being proportional to the difference between the equilibrium slope β_e and the actual local slope in the local cross-shore direction,

$$\boldsymbol{q_C} = -\gamma(\nabla z_b \cdot \hat{\mathbf{n}} + \beta_e)\hat{\mathbf{n}} \; . \tag{S8}$$

The first term describes the downslope transport and the second term simulates the net wave-induced onshore transport (Falqués et al., 2021). The third term in Eq. (S6) represents the tendency of small bumps to be flattened in the alongshore direction due to wave stirring if there is no positive feedback,

$$\boldsymbol{q_D} = -\gamma(\nabla z_b \cdot \hat{\mathbf{t}})\hat{\mathbf{t}} \; . \tag{S9}$$

The stirring factor γ in both $\boldsymbol{q_C}$ and $\boldsymbol{q_D}$ accounts for sediment stirring by currents, wave orbital velocity and turbulence. The magnitude of the horizontal momentum mixing given by Battjes (1975) is used as scaling factor,

$$\gamma = \nu \gamma_b^{-1/6} H_b^{11/6} Y_b'^{-1/3} g^{1/2} \psi(D) \; , \tag{S10}$$

where γ_b is the saturation ratio of H/D inside the surf zone (here, $\gamma_b = 0.5$), $D = z_s - z_b$ is water depth, Y_b' is the surf zone width (computed in the y' direction), g is gravity acceleration and the constant of proportionality ν is the second calibration parameter. The shape function ψ (Arriaga et al., 2017) is assumed to have a maximum value at the shoreline ($\psi(0) = 1$) and to decay both landward (across the swash zone) and seaward, being negligible at the depth of closure, D_c.

Incident monochromatic waves with $T = T_p$ (peak period), $H = H_s$ (significant wave height) and a wave angle θ are considered at the offshore boundary. Since sediment transport computation requires the wave characteristics at breaking, the waves are propagated inside the domain up to breaking point using the geometric optics approximation, i.e., applying the dispersion relation, the wave number irrotationality and the wave energy conservation (van den Berg et al., 2012; Arriaga et al., 2017). From the computed wave field, the breaker wave height, H_b, and the corresponding wave angle, θ_b, are extracted. The mean sea level, $z_s(x, y, t)$ is assumed to be uniform through all the domain except in the surf zone where a proxy for wave set-up is introduced (Ribas et al., 2023).

Given that Castell beach is an embayed beach, it is important to represent the wave shadow zones next to the lateral boundaries for off-normal wave incidence. This was not included in the previous versions of the model and has been specifically designed for this application. Following the overall rationale of the model (reduced-complexity), wave shadowing and diffraction by the lateral solid boundaries is treated in a simplified way. First, the wave field is computed as if the domain was open without solid boundaries. The "limiting wave ray", i.e., the wave ray just grazing the offshore tip of the up-waves solid wall, is determined. This defines the "shadow zone" as the area between this ray and the wall. The wave angles outside the shadow zone are kept unaltered while the angles inside the shadow are approximated by an alongshore linear interpolation between the angle corresponding to the limiting ray and 0 (shore-normal incidence) at the wall. The wave height computed by ignoring the walls, $H(x, y)$, is substituted in all the domain by $r(x, y)H(x, y)$, where $0 < r(x, y) \leq 1$ is a factor representing wave diffraction. The Sommerfeld's solution for diffraction by a semi-infinite wall on a horizontal flat bottom (Dean and Dalrymple, 2002) provides a proxy for this factor. It is 0.5 at the limiting ray, it decreases towards the wall and rapidly increases to 1 outside the shadow zone. Outside the shadow zone, the values of $r(x, y)$ that according to the Sommerfeld's solution should slightly oscillate around 1 are simply set to 1.

A shifted Dean profile (Dean, 1991; Falqués and Calvete, 2005)

$$D(y') = B((y' + y_0)^{2/3} - y_0^{2/3}) \tag{S11}$$

is used to create the equilibrium beach profile, where y' is the distance to the shoreline. The equilibrium bed slope $\beta_e = dD/dy'$ as a function of the water depth, D, is then extracted from this equation. The B and y_0 parameters are computed from the slope at the coastline, β_s, and the depth D_1 at a distance $y' = 291$ m, which controls the overall slope of the equilibrium profile. In agreement with the observed bathymetry of January 2020, the shoreline slope was fixed to $\beta_s = 0.16$ while D_1 is left as a calibration parameter.

S4 Extra figures related to the calibration of the models

In this section the figures representing the XBeach model calibration results are first shown, using the Brier Skill Score (BSS) and the Standard Deviation (σ) as metrics (described in detail in Sect. 3.3 of the main article). First, the BSS and σ of the coastline and the bathymetry for different values of the cross-shore sediment transport parameters (f_{Sk} and f_{As}) are shown in Fig. (S4. Also, the two BSS and σ obtained for different values of the Manning coefficient (n) can be seen in figure S5.

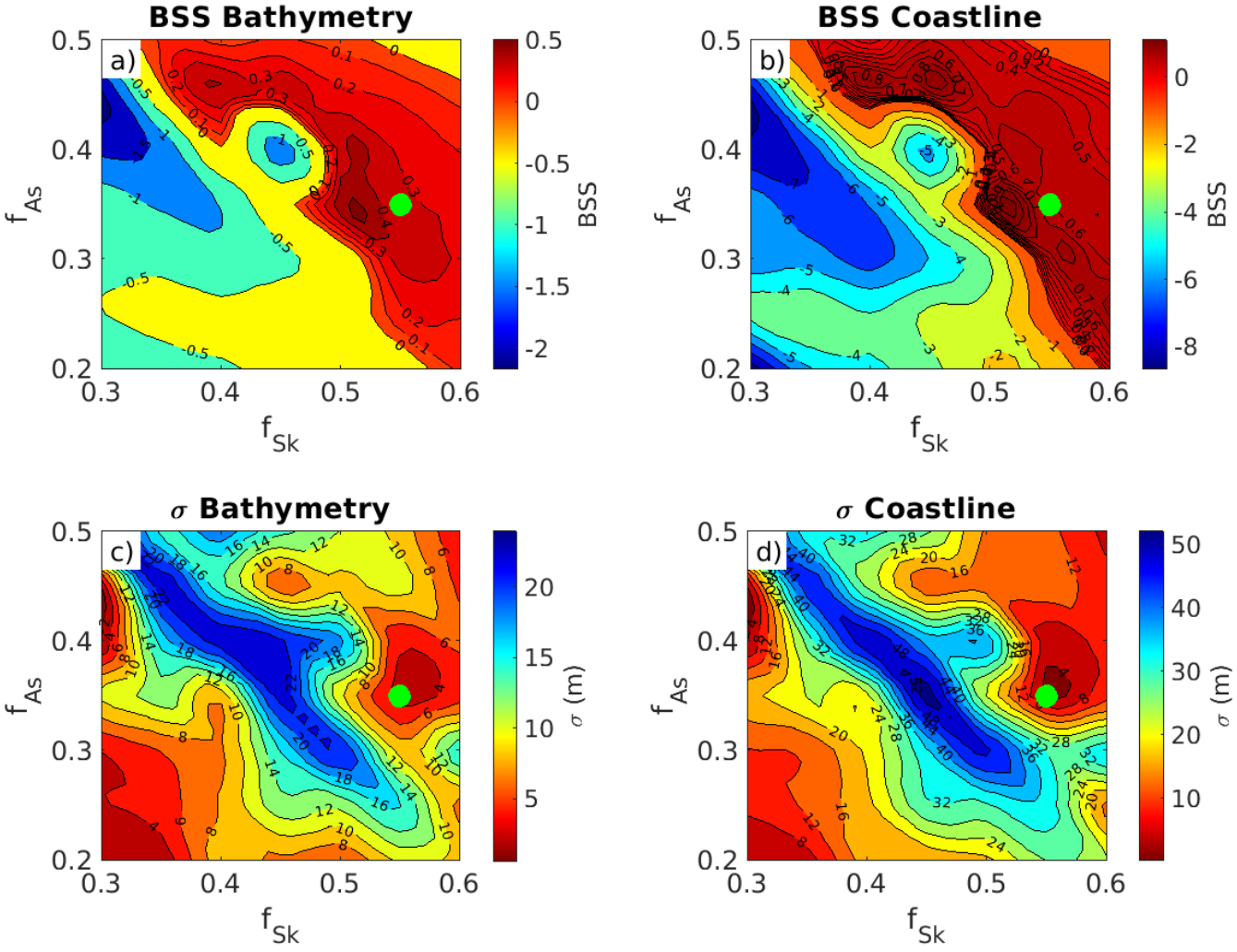

Figure S4. XBeach results obtained for the Brier Skill Score (BSS) metric of the bathymetry (a) and the coastline (b) and for the Standard deviation (σ) metric of the bathymetry (c) and the coastline (d) using all combinations of f_{Sk} and f_{As} parameters tested. The selected optimal parameter set is shown with a green dot in all panels. The calibrated values shown in Table 2 of the manuscript were used for the rest of parameters.

Finally, the figures representing the Q2Dmorfo calibration by varying the ν, μ and D_1 parameter values and the resulting coastline BSS are shown in figure S6.

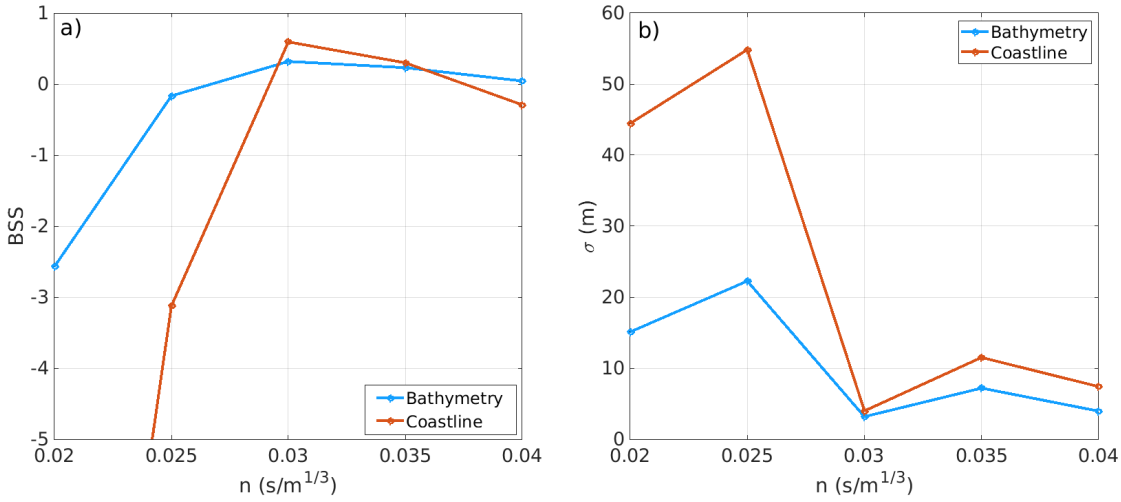

Figure S5. XBeach results obtained for the Brier Skill Score (BSS) metric (a) and for the Standard deviation (σ) metric (b) of the coastline and the bathymetry when varying the Manning coefficient n, using the optimum values $f_{Sk} = 0.55$ and $f_{As} = 0.35$. The calibrated values shown in Table 3 of the manuscript were used for the rest of parameters.

References

Arriaga, J., Rutten, J., Ribas, F., Ruessink, B., and Falqués, A.: Modeling the longterm diffusion and feeding capability of a mega-nourishment, Coast. Eng., 121, 1–13, 2017.

Bae, H., Do, K., Kim, I., and Chang, S.: Proposal of Parameter Range that Offered Optimal Performance in the Coastal Morphodynamic Model (XBeach) Through GLUE, Journal. of Ocean Engineering and Technology., 36, 251–269, https://doi.org/10.26748/KSOE.2022.013, 2022.

Battjes, J. A.: Modeling of turbulence in the surfzone, in: Proc. Symp. Model. Tech., pp. 1050–1061, Am. Soc. of Civ. Eng., New York, 1975.

De Swart, R. L., Ribas, F., Calvete, D., Kroon, A., and Orfila, A.: Optimal estimations of directional wave conditions for nearshore field studies, Continental Shelf Research, 196, 104 071, https://doi.org/doi:10.1016/j.csr.2020.104071, 2020.

Dean, R. G.: Equilibrium beach profiles: characteristics and application, J. Coastal Res., 7, 53–84, 1991.

Dean, R. G. and Dalrymple, R. A.: Coastal Processes, Cambridge University Press, Cambridge, 2002.

Falqués, A. and Calvete, D.: Large scale dynamics of sandy coastlines. Diffusivity and instability, J. Geophys. Res., 110, https://doi.org/10.1029/2004JC002587, 2005.

Falqués, A., Ribas, F., Mujal-Colilles, A., and Puig-Polo, C.: A new morphodynamic instability associated with cross-shore transport in the nearshore, Geophys. Res. Lett., 48, e2020GL091 722, 10.1029/2020GL091722, 2021.

Galappatti, G. and Vreugdenhil, C. B.: A depth-integrated model for suspended sediment transport, J. Hydraulic Research., 23, 359–377, 1985.

Horikawa, K.: Nearshore Dynamics and Coastal Processes, University of Tokio Press, Tokio, Japan, 1988.

Komar, P. D.: Beach Processes and Sedimentation, Prentice Hall, Englewood Cliffs, N.J., second edn., 1998.

Komen, G. J., Hasselmann, S., and Hasselmann, K.: On the Existence of a Fully Developed Wind-Sea Spectrum, Journal of Physical Oceanography, 14, 1271–1285, 1984.

Mitsuyasu, H., Tasai, F., Suhara, T., Mizuno, S., M, O., Honda, T., and Rikiishi, K.: Observations of the Directional Spectrum of Ocean WavesUsing a Cloverleaf Buoy, Journal of Physical Oceanography, 5, 750–760, 1975.

Ribas, F., de Swart, H. E., Calvete, D., and Falqués, A.: Modelling waves, currents and sandbars on natural beaches: the effect of surface rollers, J. Marine Syst., 88, 90–101, doi:10.1016/j.jmarsys.2011.02.016, 2011.

Ribas, F., Portos-Amill, L., Falqués, A., Arriaga, J., Marcos, M., and Ruessink, G.: Impact of mean sea-level rise on the long-term evolution of a mega-nourishment, Climatic Change, 176, 66, doi:10.1007/s10584-023-03503-6, 2023.

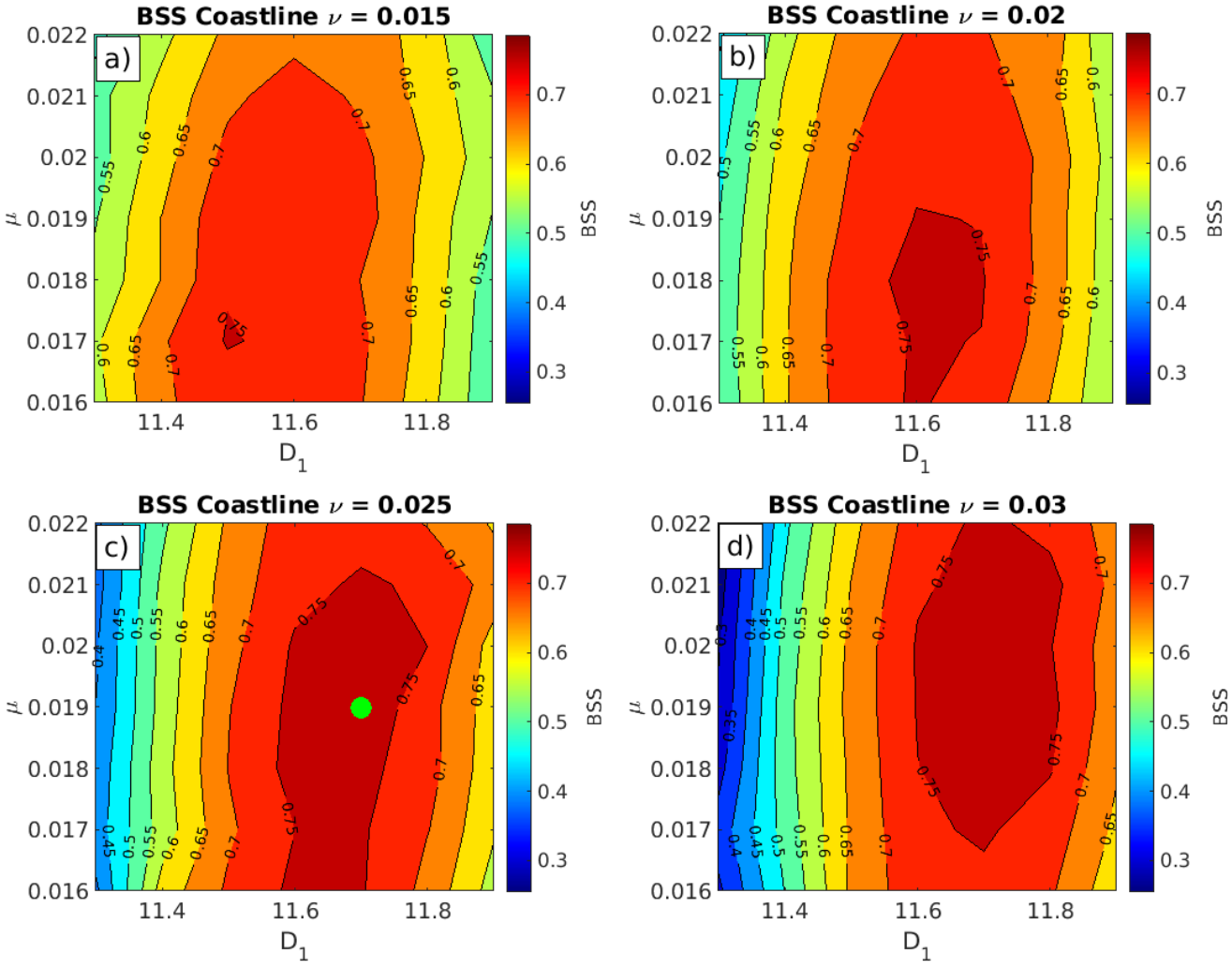

Figure S6. Q2Dmorfo results obtained for the coastline BSS for all the combinations of ν, μ and D_1 parameter values tested. The selected optimal parameter set is shown with a green dot in panel c.

Roelvink, D., Reniers, A., van Dongeren, A., de Vries, J. V. T., McCall, R., and Lescinski, J.: Modelling storm impacts on beaches, dunes and barrier islands, Coastal Engineering, 53, 1133–1152, 2009.

Roelvink, J. A. and Stive, M. J. F.: Bar-generating cross-shore flow mechanisms on a beach, J. Geophys. Res., 94, 4785–4800, 1989.

Ruessink, B. G., Miles, J. R., Feddersen, F., Guza, R. T., and Elgar, S.: Modeling the alongshore current on barred beaches, J. Geophys. Res., 106, 22 451–22 463, 2001.

Rutten, J., Torres-Freyermuth, A., and Puleo, J. A.: Uncertainty in runup predictions on natural beaches using XBeach nonhydrostatic, Coastla Engineering, 116, 2021.

Team, S.: SWAN Scientific and Technical Documentation. SWAN Cycle III Version 41.31. Tech rep., Delft, The Netherlands: Delft University of Technology, 2019a.

Team, S.: SWAN User Manual. SWAN Cycle III Version 41.31. Tech rep., Delft, The Netherlands: Delft University of Technology, 2019b.

van den Berg, N., Falqués, A., and Ribas, F.: Modelling large scale shoreline sand waves under oblique wave incidence, J. Geophys. Res., 117, https://doi.org/10.1029/2011JF002177, 2012.

van Thiel de Vries, J.: Dune erosion during storm surges, Ph.D. thesis, Delft University of Technology, Amsterdam, The Netherlands, 2009.